

# 1 **A Local Particle Filter for High Dimensional Geophysical** 2 **Systems**

3

4 **S. G. Penny<sup>1,2,3</sup> and T. Miyoshi<sup>3,1</sup>**

5 [1]{University of Maryland, College Park, Maryland, United States}

6 [2]{National Centers for Environmental Prediction, College Park, MD, United States}

7 [3]{RIKEN Advanced Institute for Computational Science, Kobe, Japan}

8 Correspondence to: S. G. Penny (Steve.Penny@noaa.gov)

9

## 10 **Abstract**

11 A local particle filter (LPF) is introduced that outperforms traditional ensemble Kalman filters  
12 in highly nonlinear/non-Gaussian scenarios, both in accuracy and computational cost. The  
13 standard Sampling Importance Resampling (SIR) particle filter is augmented with an  
14 observation-space localization approach, for which an independent analysis is computed  
15 locally at each gridpoint. The deterministic resampling approach of Kitagawa is adapted for  
16 application locally and combined with interpolation of the analysis weights to smooth the  
17 transition between neighboring points. Gaussian noise is applied with magnitude equal to the  
18 local analysis spread to prevent particle degeneracy while maintaining the estimate of the  
19 growing dynamical instabilities. The approach is validated against the Local Ensemble  
20 Transform Kalman Filter (LETKF) using the 40-variable Lorenz-96 model. The results show  
21 that: (1) the accuracy of LPF surpasses LETKF as the forecast length increases (thus  
22 increasing the degree of nonlinearity), (2) the cost of LPF is significantly lower than LETKF  
23 as the ensemble size increases, and (3) LPF prevents filter divergence experienced by LETKF  
24 in cases with non-Gaussian observation error distributions.

25

26

# 1    **1    Introduction**

2    The Particle Filter (PF) has been explored in the data assimilation community since the  
3    introduction of its Gaussian linear variant, the Ensemble Kalman Filter (EnKF) in the mid-  
4    1990's (*Evensen, 1994*). While general PFs have been intractable for high dimensional  
5    systems, the EnKF has experienced great success in numerical weather prediction (NWP)  
6    (*e.g. Kleist 2012; Hamrud et al., 2014*) and ocean data assimilation (*e.g. Penny et al. 2015*).  
7    However, at least two limitations are on the horizon for EnKFs. Perhaps counter-intuitively,  
8    these limitations arise due to *increased* computational resources, and have already become  
9    challenges at the RIKEN Advanced Institute for Computational Science (AICS, *e.g.*,  
10    *Miyamoto et al. 2013; Miyoshi et al. 2014; 2015*). First, global models will be pushed to  
11    higher resolutions in which they begin to resolve highly nonlinear processes. To maintain the  
12    Gaussian linear assumption required for the EnKF, much smaller timesteps are needed. For  
13    example, the standard 6-hour analysis cycles used for the atmosphere may need to be  
14    decreased to 5 minutes or even 30 seconds. Second, large ensembles (*e.g.* with ensemble size  
15     $k > 10,000$  members) will become feasible for lower-resolution models. While at first this  
16    may seem an advantage rather than a limitation, the computational cost of the local ensemble  
17    transform Kalman filter (LETKF) (*Hunt et al., 2007*), for example, increases at a rate  $O(k^3)$   
18    with the ensemble size  $k$ . Thus as the ensemble size increases, the cost of computing the  
19    analysis increases at a much greater rate. Alternative EnKFs feasible for large geophysical  
20    systems scale in computational cost with the observation dimension, which is typically  
21    multiple orders of magnitude larger than the ensemble dimension.

22    The PF is generally applicable to nonlinear non-Gaussian systems, including cases with multi-  
23    modal distributions or nonlinear observation operators. With little difficulty, PFs can  
24    explicitly include representation of model error, nonlinear observation operators (*Nakano*  
25    *2007; Lei and Bickel 2011*), non-diagonal observation error covariance matrices, and non-  
26    Gaussian likelihood functions. For example, observed variables such as precipitation are  
27    inherently non-Gaussian and cannot be effectively assimilated by standard EnKF techniques  
28    (*e.g. Lien et al. 2013; 2015*). In the expansion to sea-ice and land data assimilation  
29    applications, the non-Gaussian quantities such as ice concentration, ice thickness, snow cover,  
30    and soil moisture outnumber those that can be modeled with Gaussian error. *Bocquet et al.*  
31    (*2010*) further review the difficulties using observations with non-Gaussian error  
32    distributions. All of these problem-specific variations can create great difficulties for standard

1 methods, such as the EnKF or variational approaches (3D-Var/4D-Var), as used in current  
2 operational systems.

3 Sampling Importance Resampling (SIR) (also known as the bootstrap filter, *Gordon et al.,*  
4 *1993*) is a commonly used enhancement to the basic Sequential Importance Sampling (SIS)  
5 particle filter. However, even with resampling the number of ensemble members required by  
6 the SIR particle filter to capture the high probability region of the posterior in high-  
7 dimensional geophysical applications is too large to make SIR usable (*Ades and van Leeuwen*  
8 *2013*). *Snyder et al. (2008)* found that the number of required ensemble members scales  
9 exponentially with the size of the system, giving the example that a 200 dimensional system  
10 would require  $10^{11}$  members. However, *Snyder et al.* note that clever choices of the proposal  
11 distribution could overcome the need for these exponentially large ensemble sizes in high-  
12 dimensional systems, which has been more recently explored by *Snyder et al. (2015)*.  
13 Applying such an approach, *van Leeuwen (2003)* considers a model for the Agulhas Current  
14 with dimension of roughly  $2 \times 10^5$ . Further, *Beskos et al. (2012)* discuss recursive methods for  
15 estimating the proposal densities, similar to the Running-in-Place algorithm (*Yang et al.*  
16 *2012a/b, Penny et al. 2013*) that has been used with LETKF in meteorological and  
17 oceanographic data assimilation. *Xiong et al. (2006)* presented techniques related to the ETKF  
18 that may provide an alternative approach to the common SIR method for generating particle  
19 estimates for the posterior distribution.

20 Techniques such as localization and inflation are typically applied as modifications to make  
21 the EnKF operationally feasible. Inspired by this practice, we introduce a local particle filter  
22 (LPF) designed for geophysical systems that is scalable to high dimensions and has  
23 computational cost  $O(k)$ . Spatial localization is typically justified by the fact that long  
24 distance correlations are either spurious or weak in comparison to nearby correlations,  
25 particularly when the ensemble is under-sampled. We use this same approach to reduce the  
26 required ensemble size for the LPF. The findings of *Jardak et al. (2000)* indicate that the  
27 EnKF with localization works well in the case of a linear observation operator but has  
28 difficulties with nonlinear observation operators.

## 29 **2 Methodology**

30 Localization is used in most operational NWP data assimilation systems, either through a  
31 direct scaling of the background error covariance matrix (*e.g. Whitaker and Hamill, 2002*) or  
32 by a scaling of the observation error covariance matrix (*Hunt et al. 2007*). Because the

1 computation of a background error covariance matrix is not needed for the PF, the latter  
 2 approach is applied here to develop an effective PF for high-dimensional geophysical  
 3 systems. Localization reduces the dimensionality of the solution space, thus requiring fewer  
 4 ensemble members to sample the phase space. Gaussian noise is applied as an additive  
 5 inflation to prevent particle degeneracy.

## 6 **2.1 The Standard SIR Particle Filter**

7 There are many variations of the PF (*Stewart and McCarty, 1992; Gordon et al., 1993;*  
 8 *Kitagawa, 1996; Hurzeler and Kunsch, 1998; Liu and Chen, 1998*). In essence it is simply a  
 9 Monte Carlo estimation of Bayes Theorem, reformulated as a recursion (*Doucet et al., 2001*),

$$10 \quad p(\mathbf{x}_t | \mathbf{y}_{1:t}) = \frac{p(\mathbf{y}_t | \mathbf{x}_t) p(\mathbf{x}_t | \mathbf{y}_{1:t-1})}{p(\mathbf{y}_t | \mathbf{y}_{1:t-1})}, \quad (1)$$

11 where  $p(x_t | y_{1:t})$  is the probability of the state  $x$  at time  $t$ , given all observations  $y$  up to time  $t$ .  
 12 We consider the model domain to be described by vectors  $x$  with dimension  $m$ , the  
 13 observation domain to be described by vector  $y$  with dimension  $l$ , and an ensemble of size  $k$ .  
 14 The term in the numerator can be expressed using the Chapman-Kolmogorov equation as,

$$15 \quad p(\mathbf{x}_t | \mathbf{y}_{1:t-1}) = \int p(\mathbf{x}_t | \mathbf{x}_{t-1}) p(\mathbf{x}_{t-1} | \mathbf{y}_{1:t-1}) dx_{t-1}, \quad (2)$$

16 and similarly the term in the denominator can be expressed as,

$$17 \quad p(\mathbf{y}_t | \mathbf{y}_{1:t-1}) = \int p(\mathbf{y}_t | \mathbf{x}_t) p(\mathbf{x}_t | \mathbf{y}_{1:t-1}) dx_t. \quad (3)$$

18 The two factors in the numerator of Equation (1) are sampled using a numerical model  $f$ ,

$$19 \quad p(\mathbf{x}_t | \mathbf{y}_{1:t-1}) \approx \frac{1}{k} \sum_{i=1}^k \delta(\mathbf{x}_t - f(\mathbf{x}_{t-1}^i)), \quad (4)$$

$$20 \quad p(\mathbf{y}_t | \mathbf{x}_t) = g(\mathbf{y}_t | \mathbf{x}_t). \quad (5)$$

21 The term in eqn. (5) is typically called the likelihood, because the probability of  $y$  given  $x$  is  
 22 equivalent to the likelihood of  $x$  given  $y$ , i.e.  $p(\mathbf{y} | \mathbf{x}) \equiv \ell(\mathbf{x} | \mathbf{y})$ . The function  $g$  is general and  
 23 can represent any distribution for the observations.

1 For the experiments here we generate two experiment cases, each with a different likelihood  
 2 function. First we use a Gaussian likelihood function corresponding to that used for EnKFs,

$$3 \quad g(\mathbf{y}_t | \mathbf{x}_t) = \frac{1}{\sqrt{(2\pi)^m |\mathbf{R}|}} \exp \left[ -\frac{1}{2} (\mathbf{y}_t - h(\mathbf{x}_t))^T \mathbf{R}^{-1} (\mathbf{y}_t - h(\mathbf{x}_t)) \right], \quad (6)$$

4 where the function  $h$  is a general, possibly nonlinear, observation operator mapping from the  
 5 model state space to the observation space. For the LPF, it is straightforward to generalize to  
 6 arbitrary non-Gaussian likelihood functions. As an example, we also apply a multivariate  
 7 Gaussian mixture model (GM<sub>2</sub>) following *Fowler and van Leeuwen (2013)* with pdf,

$$8 \quad p(\mathbf{y} | \mathbf{x}) \propto \nu_w \exp \left[ (\mathbf{y} + \nu_1 \mathbf{1} - h(\mathbf{x}))^T \mathbf{R}^{-1} (\mathbf{y} + \nu_1 \mathbf{1} - h(\mathbf{x})) \right] \\
 + (1 - \nu_w) \exp \left[ (\mathbf{y} + \nu_2 \mathbf{1} - h(\mathbf{x}))^T \mathbf{R}^{-1} (\mathbf{y} + \nu_2 \mathbf{1} - h(\mathbf{x})) \right]. \quad (7)$$

9 Let each ensemble member be identified with an index,  $i$ . Normalized weights are evaluated  
 10 for each member,

$$11 \quad w_t^i = \frac{p(\mathbf{y}_t | \mathbf{x}_t^i)}{\sum_{j=1}^k p(\mathbf{y}_t | \mathbf{x}_t^j)}. \quad (8)$$

12 Then the posterior is,

$$13 \quad p(\mathbf{x}_t | \mathbf{y}_{1:t}) \approx \sum_{i=1}^k w_t^i \delta(\mathbf{x}_t - f(\mathbf{x}_{t-1}^i)). \quad (9)$$

14 Based on Liouville's theorem, the evolution of a probability measure in a dynamical system  
 15 satisfies the property that "the probability of finding trajectories inside the time-variant  
 16 volume  $W(t)$  is constant during the evolution of the dynamical system." (Property 2,  
 17 [http://www.ulb.ac.be/di/map/gbonte/ftp/bontempi\\_fpde.pdf](http://www.ulb.ac.be/di/map/gbonte/ftp/bontempi_fpde.pdf)). If the solution manifold expands  
 18 in some directions, so will the pdf represented by the particles. Thus, the fidelity of the  
 19 distribution will quickly become insufficient to sample a solution manifold around the true  
 20 trajectory. A resampling procedure is used to refocus the particles on the densest areas of the  
 21 distribution at each analysis step. For the experiments here, we use a resampling procedure  
 22 that resembles resampling with replacement. After resampling we have,

$$p(\mathbf{x}_t | \mathbf{y}_{1:t}) \approx \frac{1}{k} \sum_{i=1}^k \delta(\mathbf{x}_t - \mathbf{x}_t^i) \quad (10)$$

## 2.2 The Transform Interpretation

The PF can be interpreted similarly to the Ensemble Transform Kalman Filter (ETKF) of Bishop et al. (2001). The transform interpretation has been explored by Reich 2013 and Metref et al. 2014. Namely we define the PF solution as a transformation of the background ensemble to the analysis ensemble,

$$\mathbf{X}^a = \mathbf{X}^b \mathbf{T} \quad (11)$$

where each column of  $\mathbf{X}^b$  is a background ensemble member, and each column of  $\mathbf{X}^a$  is an analysis ensemble member. The transform function  $\mathbf{T}$  in (11) is used to generically refer to either  $\mathbf{E}$  in (16), or  $\mathbf{E}^{(i)}$  in (19) in the text below.

Let  $\mathbf{b}$  be the vector of background particle indices and  $\mathbf{a}$  be the vector of analysis particle indices,

$$\mathbf{b} \in \left\{ \mathbf{z} \in \mathbb{Z}^k \mid \mathbf{z} = (1, 2, 3, \dots, k)^T \right\}, \quad (12)$$

$$\mathbf{a} \in \left\{ \mathbf{z} \in \mathbb{Z}^k \mid \mathbf{z} = (a_1, a_2, a_3, \dots, a_k)^T, a_i \in [1, k] \right\}. \quad (13)$$

Here,  $\mathbf{b}$  is simply vector composed of an ordered set of indices ranging from 1 to  $k$ , while  $\mathbf{a}$  is a vector composed of a subset of elements of the vector  $\mathbf{b}$ , with no particular ordering and possible repetitions. We also extend the definition of  $\mathbf{a}$  to allow the vector to vary by grid point. For example, for any grid point  $p$ , the vector  $\mathbf{a}_p$  may represent the resampling index at point  $p$  so that,

$$\mathbf{X}^a(p, i) = \mathbf{X}^b(p, a_{p,i}), \quad (14)$$

where the arguments indicate the row and column of the matrix  $\mathbf{X}$ .

We further define the vector  $\mathbf{e}_i$ , for which only the  $i^{\text{th}}$  element is nonzero,

$$\mathbf{e}_i \in \left\{ \mathbf{z} \in \mathbb{Z}_2^k \mid \mathbf{z} = (0, \dots, 0, 1_i, 0, \dots, 0)^T \right\}. \quad (15)$$

If  $\mathbf{e}_i$  are the canonical basis vectors then we can define,

$$\mathbf{E}_{k \times k} = \begin{bmatrix} \mathbf{e}_{a_1} & \mathbf{e}_{a_2} & \cdots & \mathbf{e}_{a_k} \end{bmatrix}. \quad (16)$$

For the standard PF, the indicator matrix  $\mathbf{E}$  is made up of  $k$  (not necessarily unique) standard basis vectors  $\mathbf{e}_i$ , with entries 0 and 1 that we will interpret as weights. Thus the analysis ensemble for the PF is defined simply by the transform,

$$\mathbf{X}_{m \times k}^a = \mathbf{X}_{m \times k}^b \mathbf{E}_{k \times k}. \quad (17)$$

We note that by using this approach, each new analysis member, with index  $i$ , maintains the continuity properties of its associated background member,  $a_i$ .

For reference in the next section, the components of the analysis matrix  $\mathbf{X}^a$  will have the form,

$$\mathbf{X}^a = \begin{bmatrix} x_{1,i} e_{i,1} & x_{1,i} e_{i,2} & \cdots & x_{1,i} e_{i,k} \\ x_{2,i} e_{i,1} & x_{2,i} e_{i,2} & \cdots & x_{2,i} e_{i,k} \\ \vdots & \vdots & \ddots & \vdots \\ x_{m,i} e_{i,1} & x_{m,i} e_{i,2} & \cdots & x_{m,i} e_{i,k} \end{bmatrix}. \quad (18)$$

Here we have used the Einstein tensor notation for the elements, in which  $x_{1,i} e_{i,1}$  represents a summation over the index  $i$  (i.e. the inner product of row 1 of  $\mathbf{X}^b$  and column 1 of  $\mathbf{E}$ ). While the summation index could be represented generically by any symbol, we reuse the symbol ' $i$ ' due to its correspondence with the background particle indices as defined above.

### 2.3 The Localization Approach

*Snyder et al. (2008)* note that when either the model dimension or observation count is large, the PF requires significantly more particles to give an adequate representation of the system. Localization, as introduced by Houtekamer and Mitchell (1998), reduces both the model and observation dimensions by dividing the problem into a series of sub-domains, thus reducing the required number of particles for accurate filtering. Bengtsson et al. (2003) were among the first to point to spatially local updating, using a local subset of observations, as a solution to difficulties of high-dimensional non-Gaussian filtering. *Lei and Bickel (2011)* introduced the notion of computing local weights in a non-Gaussian filter. The LPF follows *Hunt et al. (2007)* to select nearby observations for independent analysis at each grid point. Nearby grid points thus assimilate nearly identical sets of observations to derive their analyses.

1 We use the deterministic resampling of *Kitagawa (1996)*, with complexity  $O(k)$ ,  
 2 adapted for local use as described next. A uniform partition of  $[0,1]$  with width  $1/k$  is first  
 3 generated globally, with an offset applied from a uniform distribution over  $[0,1/k]$ . The same  
 4 partition is used locally for resampling at each grid point. Cumulative sums of the normalized  
 5 weights (eqn. 8),

$$6 \quad \tilde{w}_t^j = \sum_{i=1}^j w_t^i, \quad (19)$$

7 are compared with the elements of the partition. Traversing  $j=1, \dots, k$  all unassigned particles  
 8 with index  $j$  having a corresponding cumulative sum with index  $j$  that surpasses the next  
 9 element of the partition (ordered monotonically increasing) are assigned as particles of the  
 10 resampled (analysis) ensemble.

11 For a given grid point, when the cumulative sums of the particle weights are near one  
 12 of the partition values, there may be sensitivity in neighboring grid points that lead to  
 13 discontinuities between local analyses. The analysis ensemble at this grid point consists of a  
 14 subset of background particle indices (1 through  $k$ ) with repetitions. To eliminate the  
 15 discontinuities with neighboring grid points we associate weights of a local transform  
 16 function  $T$  with the particle indices, nominally either 1.0 (full weight) or 0.0 (no weight). This  
 17 is partially inspired by the “weight interpolation” of *Bowler (2006)*, applied to LETKF by  
 18 *Yang et al. (2009)*, who found that interpolation of weights was more robust than interpolation  
 19 of state values. At a single grid point, there are  $k$  pieces of background information about the  
 20 possible system state at that point. In the standard PF, only 1 out of these  $k$  pieces of  
 21 information is retained for each analysis ensemble member, based on the overall agreement  
 22 with observations. In the LPF we use anywhere from 1 to  $k$  members to construct each  
 23 analysis member based on the agreement with observations within a local radius.

24 Thus the modified local analysis at a given model grid point  $p$  is given as a linear  
 25 combination of ensemble members at that point. For point  $p$ , ensemble member  $i$ , a set of  $N$   
 26 neighbor points  $N_p$ , and vector  $\mathbf{a}_p$  acting as a resampling index as in (13) but given as a  
 27 function of the model grid point, we have,

$$28 \quad \mathbf{X}_{\{p,i\}}^{LPF} = \frac{1}{2} \mathbf{X}_{\{p,i\}}^a + \frac{1}{2N} \sum_{n \in N_p} \mathbf{X}_{\{p,\mathbf{a}(n,i)\}}^b. \quad (20)$$

29 The subscript indices indicate the row and column of the matrix.



1 A new transform can then be defined for the LPF at each point in the model domain to  
 2 generate a set of  $m$  indicator matrices,  $\mathbf{E}_{k \times k}^{(j)}$ , so that for each point ( $x_p$ , for  $p=1, \dots, m$ ),

$$3 \quad (\mathbf{X}_{m \times k}^a)^p = \mathbf{X}_{m \times k}^b \mathbf{E}_{k \times k}^{(p)}. \quad (21)$$

4 Using the summation tensor notation described in the previous section, the analysis ensemble  
 5 can be written,

$$6 \quad \mathbf{X}^a = \begin{bmatrix} x_{1,i} e_{i,1}^{(1)} & x_{1,i} e_{i,2}^{(1)} & \cdots & x_{1,i} e_{i,k}^{(1)} \\ x_{2,i} e_{i,1}^{(2)} & x_{2,i} e_{i,2}^{(2)} & \cdots & x_{2,i} e_{i,k}^{(2)} \\ \vdots & \vdots & \ddots & \vdots \\ x_{m,i} e_{i,1}^{(m)} & x_{m,i} e_{i,2}^{(m)} & \cdots & x_{m,i} e_{i,k}^{(m)} \end{bmatrix}. \quad (22)$$

7 The transform matrix may have any degree of sophistication. We apply a smoothing operator  
 8 to the ensemble subspace by modifying the weights  $\mathbf{e}_{a_i}$  associated with each analysis particle  
 9 index  $\mathbf{a}_{(i)}$  from a binary value to a continuous value between 0 and 1, while maintaining all  
 10 column sums of equal to one, and call this new transform matrix  $\mathbf{W}$ .

11 We define the concept of a ‘neighbor point’ abstractly as a point near the analyzed grid  
 12 point based on a specified distance metric. Through examination of (20), it is clear that the  
 13 choice of neighbor points simply informs the weighting of indices, and that the values at these  
 14 neighbor points otherwise have no impact on the analysis. If there are  $N$  neighbor points, then  
 15 there will be at most  $\min(N+1, k)$  collocated pieces of background information that can be  
 16 utilized to construct each analysis ensemble member at this point. An example is given in  
 17 **Figure 1**. With a sufficiently large set of observations the indices for these neighbor points  
 18 are calculated from nearly identical observational innovations. Therefore, when there is a  
 19 sufficiently large ensemble size ( $k$ ) the difference between the states associated with different  
 20 particle indices will be small. The transform function  $T$  is applied across all background  
 21 indices (i.e. for particles  $1, \dots, k$ ) at this grid point to compute the analysis.

22 We summarize that the total smoothing in the resulting analysis is achieved  
 23 independently at each grid point due to a combination of localization in observation space and  
 24 the formation of a convex combination of analysis weights in the ensemble space. There is no  
 25 explicit smoothing in the physical model space such as might occur using a Gaussian  
 26 smoother applied via a stencil of function values from neighboring grid points. Instead, the

1 neighbor points simply inform the choice of weights to apply to particle indices at a single  
2 grid point. There is an implicit smoothing achieved by applying the same procedure to many  
3 contiguous model grid points, each generating a different set of weights that vary only  
4 slightly. This is similar to the effect of observation-space localization. However, as with most  
5 localization techniques, the more distant information suffers from the poor sampling size of  
6 the ensemble. Thus if holding the ensemble size  $k$  fixed, a larger radius of neighbor points  
7 may lead to noisier results rather than increased smoothing.

## 8 **2.4 Particle Degeneracy**

9 The particle selection process of the PF reduces the rank of the ensemble. For a linear  
10 deterministic system this leads to a rapid collapse of the ensemble and divergence of the filter.  
11 For a sufficiently stochastic nonlinear system the members are made distinct after a single  
12 forecast step. If the nonlinear system is not sufficiently stochastic, then we must address the  
13 ensemble initialization problem at every analysis cycle. *Pazo et al. (2010)* discuss the  
14 desirable properties in an initial ensemble, namely the members: (1) should be well-embedded  
15 in the attractor, (2) should be statistically equivalent but have enough diversity to represent a  
16 significant portion of the phase space, (3) should adequately represent the error between the  
17 analysis and true state, and (4) should sample the fastest growing directions in phase space.  
18 We wish to avoid particle degeneracy while also engendering some of these qualities.  
19 Applying noise to the PF at the sampling step is a common empirical technique. Therefore we  
20 employ a simple approach: at each cycle we add Gaussian noise with variance scaled locally  
21 to a magnitude matching the analysis error variance and apply this to each analysis member  
22 prior to the subsequent ensemble forecast. The amplitude of the additive noise was chosen to  
23 conform to the dynamics of the growing error subspace, as estimated by the analysis  
24 ensemble spread. We note that this amplitude varies spatially and temporally. The results  
25 degraded when departing from this approach. The practice of applying noise to the PF  
26 sampling step is a standard technique.

27 We caution that EnKFs have fundamentally different behavior than the general PF, in  
28 that the former maintain a forcing term that drives the DA system toward the observations  
29 even when the forecast may start far from the true state. The general PF with resampling  
30 essentially requires random chance to generate a state with high enough probability to be  
31 propagated through the resampling step. As the system size increases and the number of  
32 particles is held fixed, the probability of such an event declines. This is connected with the

1 divergence of the PF when there are insufficient particles, which has been explored in detail  
 2 by *Snyder et al. (2008)*.

### 3 **2.5 Computational Complexity**

4 A data assimilation system is comprised of many components. We simplify the cost analysis  
 5 in order to gain an approximate relative measure of the algorithms presented here. Let  $m$  be  
 6 the model dimension,  $l$  be the observation dimension, and  $\bar{l}_i$  be the average local observation  
 7 dimension. The total cost ( $C_T$ ) of an analysis cycle is equal to the overhead ( $C_H$ ) of the  
 8 assimilation system plus  $m$  times the average local cost ( $C_L$ ) of the assimilation method plus  $k$   
 9 times the cost of one model forecast ( $C_M$ ) of duration  $t$ ,

$$10 \quad C_T(k, l, m) = C_H(k, l, m) + m \cdot C_L(k, \bar{l}_i) + k \cdot C_M(\tau, m) \quad (23)$$

11 We will assume that between the two methods the overhead and model costs are  
 12 approximately equal. The primary difference in cost between the two systems is then the  
 13 average local cost,

$$14 \quad C_L^{LPF} = O(k\bar{l}_i), \quad (24)$$

$$15 \quad C_L^{LETKF} = O(k^2\bar{l}_i + k^3). \quad (25)$$

16 If as is typically the case, the system size  $m$  is large and the ensemble size  $k$  is small, then

$$17 \quad C_T(k, l, m) \approx C_H(k, l, m) + O(m), \quad (26)$$

18 and the difference in cost between LETKF and LPF is small. However for large  $k$ , we see that  
 19 the average local cost of LETKF,

$$20 \quad C_T^{LETKF}(k, l, m) = C_H(k, l, m) + O(mk^3), \quad (27)$$

21 exceeds that of the LPF,

$$22 \quad C_T^{LPF}(k, l, m) = C_H(k, l, m) + O(mk). \quad (28)$$

23 Subtracting the overhead costs, in this case the LPF is a factor of  $k^2$  cheaper than LETKF.

## 1 **2.6 Data Assimilation Methods**

2 We enumerate the benefits of the LPF versus the benchmark LETKF, an ensemble square root  
3 filter that performs its analysis in the ensemble space at each grid point using a geospatially  
4 local selection of observations. The LETKF approach is very efficient as long as the ensemble  
5 size is small relative to the number of observations and the model dimension.

6 We use LETKF as a proxy for a general EnKF. *Nerger (2015)* gives a comparison between  
7 LETKF and the Ensemble Square Root Filter (ESRF) of *Whitaker and Hamill (2002)*, while  
8 *Tippett et al. (2003)* indicate that the ESRF is identical to the Ensemble Adjustment Kalman  
9 Filter (EAKF) of *Anderson (2001)* when using serial single observation processing.

## 10 **2.7 Experiment Design**

11 We demonstrate the algorithms on the Lorenz-96 system (*Lorenz 1996*), composed of  $m=40$   
12 grid points, using Lorenz's original forcing,  $F=8.0$ . The Lorenz-96 system has frequently been  
13 used to demonstrate PF and other data assimilation algorithms for the geosciences (*Nakano et*  
14 *al, 2007; van Leeuwen, 2010; Lei and Bickel, 2011; Penny 2014*). Observations are sampled  
15 from a nature run of Lorenz-96 after running the model for 14,400 timesteps to allow the  
16 model to settle on the attractor. Gaussian noise is added to each observation with a standard  
17 deviation of 0.5. For various experiments, the Lorenz-96 system is observed either at every  
18 0.05 or 0.5 timesteps, reflective of a 6-hour and 60-hour forecast, respectively, based on  
19 Lorenz's original description of the system. Observations are sampled randomly on the  
20 interval  $[0,m]$ , and a linear interpolation is used for the observation operator. The last  
21 experiment case uses a bimodal Gaussian mixture distribution to represent observational  
22 error.

## 23 **3 Results**

24 The standard SIR PF performs poorly with any ensemble size  $O(m)$ . For example, using 1500  
25 particles and 20 randomly chosen observations per analysis cycle leads to rapid filter  
26 divergence for the L96 system, even in a relatively linear regime ( $dt=0.05$ ) of the system  
27 (**Figure 2**). On the contrary, LETKF performs well even with few ensemble members and few  
28 observations per cycle ( $k=20, l=10$ ). Localization is consistent between each method, using  
29  $r=2$  gridpoints. For a given ensemble size, increasing the localization radius degraded the  
30 accuracy of both methods. Penny (2014) addressed the impact of varying localization radius  
31 on LETKF for this L96 system. It was shown that for a fixed ensemble size, the analysis

1 errors reduce when the localization radius decreases, and for a fixed localization radius, the  
2 analysis errors reduce when the ensemble size increases. The LPF showed similar behavior to  
3 LETKF in this regard. To explore the relative advantages of each approach, we will describe a  
4 series of cases in which the LETKF outperforms the LPF, and in which the LPF outperforms  
5 LETKF.

### 6 **3.1 Case 1: typical forecast lengths ( $dt=0.05$ , or 6-hr)**

7 *Lorenz (1996)* introduced the  $dt=0.05$  timescale as being comparable to the error doubling  
8 taking place over 6 hours in the operational forecasting systems of the early 1990's. In this  
9 relatively linear timescale of the L96 system, LETKF clearly outperforms the LPF at a given  
10 ensemble size. This is expected as EnKFs take advantage of the Gaussian/linear assumption.  
11 When the experiment parameters match such assumptions (even loosely), LETKF performs  
12 quite well. However, using localization, the LPF can perform adequately (i.e. avoid filter  
13 divergence) in a similar parameter regime (**Figure 3**). Thus for this case, we find that LETKF  
14 attains higher accuracy than the LPF, but the LPF improves upon the accuracy and stability of  
15 the standard SIR PF for a given ensemble size.

### 16 **3.2 Case 2: long forecast lengths ( $dt=0.50$ , or 60-hr)**

17 To increase the degree of nonlinearity in a data assimilation system using L96, it is typical to  
18 increase the analysis cycle length (e.g. *Lei and Bickel, 2011*). The LPF has superior  
19 performance for more nonlinear regimes of the L96 system (e.g.  $dt=0.5$ ) provided there are  
20 many ensemble members, e.g.  $O(100)$ . Using 80 observations per cycle and 100 ensemble  
21 members, for example, LETKF produces occasional errors that propagate eastward (along the  
22 positive x-direction). The LPF does not produce such effects, and the errors are generally  
23 lower than with LETKF (**Figure 4**). We consider this a relevant scenario because the majority  
24 of observations in operational weather forecasting are discarded (*Ochatta et al., 2005*).

25 Exploring a more complete parameter space, we examine the forecast error for LETKF  
26 over a range of observation coverage ( $l=2, \dots, 80$  per analysis cycle) and ensemble sizes  
27 ( $k=10, \dots, 400$ ), and compare the relative difference to LPF. **Figure 5** shows the average  
28 absolute error over 600 analysis cycles of length  $dt=0,5$  for 1600 different parameter  
29 combinations of observation coverage ( $l$ ) and ensemble size ( $k$ ). The LPF is more accurate

1 than LETKF when using many observations (e.g.  $l > 20$ ) and large ensemble sizes (e.g.  $k >$   
2 100-200).

3 When using fewer than 20 observations per cycle in this case, both LETKF and LPF  
4 experience filter divergence. Due to the unconstrained nature of the LPF as described in  
5 section 2.4, large errors occur more frequently than for LETKF in this parameter regime.  
6 Control theory concepts regarding observability indicate that with too few observations any  
7 filter will diverge. In the linear theory for autonomous systems the conditions are  
8 straightforward. For chaotic systems, the observability of a system is difficult to identify  
9 analytically. For the particular experiment parameters given here, these results indicate that  
10 the minimum number of required observations is approximately 20 observations per model  
11 equivalent of 60-hour update intervals. *Abarbanel et al. (2009)* have made analogous  
12 conclusions regarding observability using synchronization methods for L96, and *Whartenby*  
13 *et al. (2013)* for shallow water flows.

14 When examining the computational cost of the LPF versus LETKF, the relative costs  
15 reflect the analytical assessment given above in section 2.5. Namely, the elapsed time of the  
16 LETKF experiments grows with the cube of the ensemble size, while the elapsed time of the  
17 LPF is significantly lower at large ensemble sizes (**Figure 6**).

### 18 **3.3 Case 3: Non-Gaussian observation error.**

19 The previous section examined the impacts of nonlinearity and non-Gaussianity on the  
20 forecast. We now examine the impacts of non-Gaussian observation error. Using a  
21 multivariate Gaussian mixture model ( $GM_2$ ) following *Fowler and van Leeuwen (2013)*, we  
22 apply a corresponding random error to the observation and compare the impacts on LETKF  
23 and LPF. We use the LETKF without modification, but modify the likelihood function of LPF  
24 to the definition of  $GM_2$  as in section 2.1, Eqn. (7). Using  $n_w=0.1$ ,  $n_l=-1$ ,  $n_2=1$ , we create a  
25 bimodal distribution biased toward the second Gaussian mode. The analysis cycle is  $dt=0.05$   
26 (6 hr) as in experiment case 1, section 3.1. **Figure 7**, compares LETKF and LPF using  $k=100$   
27 ensemble members and  $l=80$  observations. An additional results is given for LPF with  $l=20$   
28 observations. The introduction of a strong non-Gaussianity in the observation error  
29 distribution disrupts LETKF and eventually creates errors that propagate throughout the entire  
30 domain. Using the same ensemble size and observation count, the LPF gains significant

1 advantage in its ability to explicitly account for the non-Gaussian error structure of the  
2 observations. Even reducing the observation count by 75%, the LPF maintains its advantage.

### 3 **3.4 Case 4: Examining the impact of spatial smoothing.**

4 We consider the example of LPF applied to L96 with the analysis cycle  $dt=0.5$  (producing a  
5 relatively non-linear error growth), a localization radius of 2 grid points,  $k=100$  ensemble  
6 members,  $l=40$  observations per cycle, and observation error of 0.5. By applying ensemble  
7 smoothing of the weights, we find that the mean absolute forecast error (averaged over the  
8 model domain) is reduced versus a non-smoothed analysis (**Figure 8**). Increasing the search  
9 radius to 2 gridpoints for the same example case does not produce any clear benefits.

10 To evaluate the impact on ensemble quality, we consider the mean effective ensemble  
11 size  $N_{eff}$ ,

$$12 \quad N_{eff} = \left[ \sum_{i=1}^j (w_t^i)^2 \right]^{-1}, \quad (29)$$

13 with  $w_t^i$  defined as in (8). This quantity is calculated at each gridpoint and then averaged over  
14 all points for each analysis cycle. We find that the effective ensemble size is increased when  
15 using the smoothed versus the non-smoothed approach (**Figure 9**).

## 16 **4 Conclusions**

17 The Local Particle Filter (LPF) has been shown to outperform a state of the art ensemble  
18 Kalman filter (i.e. LETKF) in scenarios that violate the Gaussian/linear assumptions of the  
19 Kalman filter. We showed the advantage of the LPF when forecast is more non-linear (via  
20 longer analysis cycles, or less frequent observations), and when observation error is non-  
21 Gaussian (using a bimodal error distribution). Further, upon transitioning to large ensembles  
22 the LPF has a significant cost savings relative to LETKF.

23 The LPF maintains many of the attractive qualities that give Particle Filters (PFs)  
24 advantages over standard EnKFs. While the PF provides a means of assimilating observations  
25 with non-Gaussian errors (e.g. precipitation, sea-ice concentration), we caution that the  
26 covariances utilized by the EnKF play a critical role in constraining the unobserved variables.  
27 Thus while the LPF is not optimal for all possible data assimilation scenarios, there is great  
28 potential for the LPF to be combined with more traditional approaches to create adaptive

1 hybrid systems that can avoid catastrophic filter divergence and manage multi-modal forecast  
2 distributions, nonlinear observation operators, non-Gaussian observations.

3 We found that a large number of ensemble members (or particles) and observations  
4 are sufficient for the LPF to match or surpass the accuracy of LETKF. We found large  
5 ensemble sizes a relevant scenario for realistic systems running on large supercomputers such  
6 as the K computer at RIKEN. The use of large observation sets is relevant in operational  
7 weather forecasting as much of the dense satellite data is currently discarding in a thinning  
8 process. Further, in this parameter regime the LPF has significantly lower computational cost  
9 than LETKF.

10 In a realistic system, some mechanism is needed to drive the ensemble toward the  
11 observations in the event of the ensemble drifting away from the true state. The PF itself has  
12 no inherent mechanism to do this other than the brute force generation of more particles.  
13 There are many techniques in the PF literature for managing filter divergence, but none of  
14 them are foolproof. *Atkins et al. (2013)* presented a promising extension of the use of an  
15 importance density that may connects effectively with the existing infrastructure of  
16 variational solvers used by most operational centers. Another popular mechanism to achieve  
17 this is regularization, which uses a kernel to sample from a continuous distribution at the  
18 resampling stage.

19 Finally, while the inflation mechanism used here was effective for the Lorenz-96  
20 system, it is not adequate for more realistic atmospheric or oceanic models. For such systems,  
21 either geospatially correlated noise or stochastic physics parameterizations may be capable of  
22 performing the same function. Stochastic physics parameterizations are an active area of  
23 research, and are under development for a number of operational center models, including  
24 NCEP (*Hou et al., 2006; Hou et al, 2010; Kolczynski et al., 2015*), ECMWF (*Berner et al.,*  
25 *2009; Weisheimer et al., 2014; Watson et al., 2015*), and the Met Office (*Tennant et al., 2011;*  
26 *Sanchez et al., 2014; Shutts and Paleres, 2014; Shutts 2015*).

## 27 **Acknowledgements**

28 We gratefully acknowledge the Japan Society for the Promotion of Science (JSPS) whose  
29 FY2013 fellowship supported this work. We would also like to thank the RIKEN Advanced  
30 Institute for Computational Science (AICS) for hosting Penny.

## 31 **Appendix**



```

1  We provide pseudo-code for the LPF:
2  % INPUTS:
3  % k    :: ensemble size
4  % m    :: model dimension
5  % Yo   :: vector of global observations
6  % yo   :: vector of local observations
7  % Xb   :: background ensemble arranged as a matrix
8  % R    :: observation error covariance matrix
9  % HXb  :: Xb mapped from model space to observation space
10 %
11 % FUNCTIONS:
12 % obsloc :: finds observations local to a grid point
13 % cumsum :: cumulative sum of array
14 % sort   :: sorting of array in descending order
15 % repmat :: repeat array to form a matrix
16 %
17 % OUTPUTS:
18 % Neff  :: effective ensemble sample size
19 % Xa    :: analysis ensemble arranged as a matrix
20
21 %
22 % Specify minimum of distribution tails
23 %
24 mintail = epsilon
25
26 %
27 % Setup global comb for resampling with replacement
28 %
29 interval = 1/k
30 start = interval * random_number
31 selection_points = [start : interval : start+(k-1)*interval]
32
33 %
34 % Loop over each grid point
35 %
36 for mi=1:m
37     % Find the observation points within range of focal grid point:
38     yo = obsloc(mi,Yo,local_radius)
39
40     % Update (calculate particle weights) using desired distribution

```

```

1      % (e.g. Gaussian shown here)
2      for ki=1:k
3          likelihood(ki) =
4              exp( -0.5* (yo-HXb(:,ki))' * R^{-1} * (yo-HXb(:,ki)) )
5      end
6
7      % Protect against numerical representation problems in the tails
8      likelihood = likelihood + mintail
9
10     %
11     % Normalize the weights
12     %
13
14     % Compute the weights
15     weights = likelihood/sum(likelihood)
16
17     % Calculate effective ensemble sample size
18     Neff(mi) = 1/sum(weights.^2)
19
20     % Form cumulative distribution
21     [wts, wi] = sort(weights)
22     weight = cumsum(wts)
23
24     %
25     % Apply the comb to resample analysis members
26     %
27     j=1
28     for i=1:k
29         while selection_points(i) >= weight(j)
30             j=j+1
31         end
32
33         % Specify the resampling index rs
34         rs(mi,i)=wi(j)
35
36         % Assign background value as global analysis
37         Xa(mi,i) = Xb(mi,rs(mi,i))
38     end
39
40 end % loop over model grid points
41

```

```

1  %
2  % Apply smoothing by weights in ensemble space.
3  %
4  x = 0
5  for ki=1:k
6      for mi=1:m
7          for ni={"set of all Np neighbor points"}
8              X(mi,ki) = X(mi,ki) + Xa(mi,ki) + Xb(mi,rs(ni,ki))
9          end
10         Xa(mi,ki) = X(mi,ki)/(2*Np);
11     end
12 end
13
14 %
15 % Apply additive inflation
16 %
17
18 % Compute the analysis ensemble spread to
19 % determine amplitude of inflation needed
20 if (mean(Neff) > k/2)
21     Xstd=std(Xa,2)
22 else
23     % add a little more noise to protect
24     % against ensemble collapse
25     Xstd=max(std(Xa,2),maximum_obs_error)
26 end
27
28 % Compute Gaussian random values with standard
29 % deviation equal to analysis ensemble spread
30 rmat=randn(m,k).*repmat(Xstd,1,k)
31
32 % Apply additive inflation (and remove sample mean)
33 Xa = Xa + rmat-repmat(mean(rmat,2),1,k)
34

```

## 35 References

36 Abarbanel, H.D.I., D.R. Creveling, R. Farsian, and M. Kostuk, 2009: Dynamical State and  
37 Parameter Estimation. *SIAM J. Appl. Dyn. Syst.*, **8**(4), 1341–1381.  
38 DOI:10.1137/090749761

- 1 Ades, M., P.J. van Leeuwen, 2013: An exploration of the equivalent weights particle filter. *Q.*  
2 *J. R. Met. Soc.*, **139** (672), 820–840.
- 3 Atkins, E., M. Morzfeld, A.J. Chorin, 2013: Implicit Particle Methods and their Connection  
4 with Variational Data Assimilation. *Mon. Wea. Rev.*, **141**(6), 1786-1803.
- 5 Berner, J., G. J. Shutts, M. Leutbecher, and T. N. Palmer, 2009: A spectral stochastic kinetic  
6 energy backscatter scheme and its impact on flow-dependent predictability in the  
7 ECMWF ensemble prediction system. *J. Atmos. Sci.*, **66**, 603–626. doi:  
8 <http://dx.doi.org/10.1175/2008JAS2677.1>
- 9 Beskos, A., D. Crisan, A. Jasra, 2012: On the Stability of Sequential Monte Carlo Methods in  
10 High Dimensions. arXiv:1103.3965v2 [stat.CO].
- 11 Bocquet, M., C.A. Pires, L. Wu, 2010: Beyond Gaussian Statistical Modeling in Geophysical  
12 Data Assimilation. *Mon. Wea. Rev.*, **138**, 2997-3023. doi: 10.1175/2010MWR3164.1
- 13 Bowler, N., 2006: Comparison of error breeding, singular vectors, random perturbations and  
14 ensemble Kalman filter perturbation strategies on a simple model. *Tellus A* **58**: 538–548.
- 15 Doucet, A., N. De Freitas and N.J. Gordon, 2001: An introduction to Sequential Monte Carlo  
16 Methods, in *SMC in Practice*. [http://www.stats.ox.ac.uk/~doucet/smc\\_resources.html](http://www.stats.ox.ac.uk/~doucet/smc_resources.html)
- 17 Evenson, G., 1994: Sequential data assimilation with a nonlinear quasi-geostrophic model  
18 using Monte Carlo methods to forecast error statistics. *J. Geophys. Res.*, **99**, 10,143–  
19 10,162.
- 20 Fowler, A., P.J. van Leeuwen, 2013: Observation impact in data assimilation: the effect of  
21 non-Gaussian observation error. *Tellus A*, **65**, 20035,  
22 <http://dx.doi.org/10.3402/tellusa.v65i0.20035>
- 23 Gordon, N.J., D. Salmond and A.F.M. Smith, 1993: Novel approach to nonlinear/non-  
24 Gaussian Bayesian state estimation, *IEE Proc. F.*, vol. 140, p. 107, 1993.
- 25 Hoffman, R.N. and E. Kalnay, 1983: Lagged Average Forecasting: an Alternative to Monte  
26 Carlo Forecasting. *Tellus*, **35**, 100-118.
- 27 Hou, D., Z. Toth, Y., Zhu, 2006: A Stochastic Parameterization Scheme Within NCEP Global  
28 Ensemble Forecast System. *Am. Met. Soc.*, 18th Conference on Probability and Statistics  
29 in the Atmospheric Sciences. <http://ams.confex.com/ams/pdfpapers/101401.pdf>

- 1 Hou, D., Z. Toth, Y. Zhu, W. Yang, R. Wobus, 2010: A Stochastic Total Tendency  
2 Perturbation Scheme Representing Model- Related Uncertainties in the NCEP Global  
3 Ensemble Forecast System. *NOAA/NCEP/EMC*,  
4 [http://www.emc.ncep.noaa.gov/gmb/yzhu/gif/pub/Manuscript\\_STTP\\_Tellus\\_A\\_HOU-](http://www.emc.ncep.noaa.gov/gmb/yzhu/gif/pub/Manuscript_STTP_Tellus_A_HOU-)  
5 [1.pdf](http://www.emc.ncep.noaa.gov/gmb/yzhu/gif/pub/Manuscript_STTP_Tellus_A_HOU-1.pdf)
- 6 Hurzeler, M. and H. Kunsch, 1998: Monte Carlo approximations for general state-space  
7 models. *JCGS*.
- 8 Jardak, M., I.M. Navon, M. Zupanski, 2010: Comparison of sequential data assimilation  
9 methods for the Kuramoto-Sivashinsky equation. *Int. J. Num. Meth. in Fluids*, **62** (4), 374-  
10 402.
- 11 Kitagawa, G., 1996: Monte Carlo filter and smoother for non-Gaussian non-linear state space  
12 models. *Journal of Computational and Graphical Statistics*, vol. **5**, no. 1, pp. 1–25.
- 13 Kolczynski, W., P. Pegion, T. Hamill, J. S. Whitaker, D. Hou, Y. Zhu, and X. Zhou. 2015:  
14 Investigating a New Stochastic Physics Suite for Use in the NCEP Global Ensemble. *Am.*  
15 *Met. Soc.*, 27th Conference On Weather Analysis And Forecasting/23rd Conference On  
16 Numerical Weather Prediction.  
17 <https://ams.confex.com/ams/27WAF23NWP/webprogram/Paper273838.html>
- 18 Lei J., and P. Bickel, 2011: A Moment Matching Ensemble Filter for Nonlinear Non-  
19 Gaussian Data Assimilation. *Mon. Wea. Rev.*, **139**, 3964-3973.
- 20 Lien, G.-Y., E. Kalnay, and T. Miyoshi, 2013: Effective assimilation of global precipitation:  
21 Simulation experiments. *Tellus A*, **65**, 19915. doi:[10.3402/tellusa.v65i0.19915](https://doi.org/10.3402/tellusa.v65i0.19915)
- 22 Lien, G.-Y., T. Miyoshi, and E. Kalnay, 2015: Assimilation of TRMM Multisatellite  
23 Precipitation Analysis with a low-resolution NCEP Global Forecasting System. *Mon.*  
24 *Wea. Rev.*, doi:[10.1175/MWR-D-15-0149.1](https://doi.org/10.1175/MWR-D-15-0149.1) (accepted and available at early online  
25 releases)
- 26 Liu, J.S. and R. Chen, 1998: Sequential Monte Carlo methods for dynamic systems. *JASA*.
- 27 Miyamoto, Y., Y. Kajikawa, R. Yoshida, T. Yamaura, H. Yashiro, and H. Tomita, 2013:  
28 Deep moist atmospheric convection in a subkilometer global simulation, *Geophys. Res.*  
29 *Lett.*, **40**, doi:10.1002/grl.50944.

- 1 Miyoshi, T., K. Kondo, and T. Imamura, 2014: The 10240-member ensemble Kalman  
2 filtering with an intermediate AGCM. *Geophys. Res. Lett.*, **41**, 5264-5271,  
3 doi:10.1002/2014GL060863.
- 4 Miyoshi, T., K. Kondo, and K. Terasaki, 2015: Big Ensemble Data Assimilation in Numerical  
5 Weather Prediction. *Computer*, in press.
- 6 Nakano, S., G. Ueno, T. Higuchi, 2007: Merging Particle Filter for Sequential Data  
7 Assimilation. *Nonlin. Pr. Geophys.*, **14**, 395-408.
- 8 Nerger, L., 2015: On Serial Observation Processing in Localized Ensemble Kalman Filters.  
9 *Mon. Wea. Rev.*, **143**, 1554-1567. doi: 10.1175/MWR-D-14-00182.1
- 10 Ochatta, T., C. Gebhardt, D. Saupe, W. Wergen, 2005: Adaptive thinning of atmospheric  
11 observations in data assimilation with vector quantization and filtering methods. *QJRM*,  
12 **131**, 3427-3437.
- 13 Ott, E., B. R. Hunt, I. Szunyogh, A. V. Zimin, E. J. Kostelich, M. Corazza, E. Kalnay, D.J.  
14 Patil, J. A. Yorke, 2004: A Local Ensemble Kalman Filter for Atmospheric Data  
15 Assimilation. *Tellus A*.
- 16 Pazo, D., M.A. Rodriguez, J.M. Lopez, 2010: Spatio-temporal evolution of perturbations in  
17 ensembles initialized by bred, Lyapunov, and singular vectors. *Tellus* 62A, 10–23.
- 18 Metref, S., E. Cosme, C. Snyder, and P. Brasseur, 2014: A non-Gaussian analysis scheme  
19 using rank histograms for ensemble data assimilation. *Nonlin. Processes Geophys.*, **21**,  
20 869–885.
- 21 Penny, S. G., E. Kalnay, J.A. Carton, B.R. Hunt, K. Ide, T. Miyoshi, and G.A.  
22 Chepurin, 2013: The local ensemble transform Kalman filter and the running-in-place  
23 algorithm applied to a global ocean general circulation model, *Nonlin. Processes*  
24 *Geophys.*, **20**, 1031-1046, doi:10.5194/npg-20-1031-2013.
- 25 Penny, S.G., 2014: The Hybrid Local Ensemble Transform Kalman Filter. *Mon. Wea. Rev.*,  
26 **142**, 2139–2149. doi: <http://dx.doi.org/10.1175/MWR-D-13-00131.1>
- 27 Reich, S., 2013: A nonparametric ensemble transform method for Bayesian inference. *SIAM*  
28 *J. Sci. Comput.*, **35**, A2013–A2024, doi:10.1137/130907367.

- 1 Sanchez, C., K.D. Williams, G. Shutts, M. Collins, 2014: Impact of a Stochastic Kinetic  
2 Energy Backscatter scheme across time-scales and resolutions. *Q. J. R. Meteorol. Soc.*,  
3 **140**, 2625 – 2637.
- 4 Shutts, G., Pallarès, A.C., 2014: Assessing parametrization uncertainty associated with  
5 horizontal resolution in numerical weather prediction models. *Phil. Trans. R. Soc. A*, **372**:  
6 20130284. <http://dx.doi.org/10.1098/rsta.2013.0284>
- 7 Shutts, G., 2015: A stochastic convective backscatter scheme for use in ensemble prediction  
8 systems. *Q. J. R. Meteorol. Soc.*, in press, doi:10.1002/qj.2547
- 9 Snyder, C., T. Bengtsson, P. Bickel, J. Anderson, 2008: Obstacles to High-Dimensional  
10 Particle Filtering. *Mon. Wea. Rev.*, **136**, 4629-4640.
- 11 Snyder., C., T. Bengtsson, M. Morzfeld, 2015: Performance bounds for particle filters using  
12 the optimal proposal. *Mon. Wea. Rev.*, in press, doi: [http://dx.doi.org/10.1175/MWR-D-](http://dx.doi.org/10.1175/MWR-D-15-0144.1)  
13 [15-0144.1](http://dx.doi.org/10.1175/MWR-D-15-0144.1)
- 14 Stewart, L., P. McCarty, 1992: The use of Bayesian Belief Networks to fuse continuous and  
15 discrete information for target recognition and discrete information for target recognition,  
16 tracking, and situation assessment, in *Proc. SPIE Signal Processing, Sensor Fusion and*  
17 *Target Recognition*, vol. 1699, pp. 177-185.
- 18 Tennant, W.J., G. J. Shutts, A. Arribas, and S. A. Thompson, 2011: Using a Stochastic  
19 Kinetic Energy Backscatter Scheme to Improve MOGREPS Probabilistic Forecast Skill.  
20 *Mon. Wea. Rev.*, **139**, 1190–1206. doi: <http://dx.doi.org/10.1175/2010MWR3430.1>
- 21 van Leeuwen, P. J., 2003: A variance-minimizing filter for large-scale applications. *Mon.*  
22 *Wea. Rev.*, **131**, 2071–2084.
- 23 van Leeuwen, P. J., 2010: Nonlinear data assimilation in geosciences: an extremely efficient  
24 particle filter. *Q.J.R.Meteorol.Soc.*, **136**, 1991-1999.
- 25 Watson, P.A.G., H. M. Christensen, T. N. Palmer, 2015: Does the ECMWF IFS Convection  
26 Parameterization with Stochastic Physics Correctly Reproduce Relationships between  
27 Convection and the Large-Scale State? *J. Atmos. Sci.*, **72**, 236-242. doi: 10.1175/JAS-D-  
28 14-0252.1
- 29 Weisheimer, A., S. Corti, T. Palmer, F. Vitart, 2014: Addressing model error through  
30 atmospheric stochastic physical parametrizations: impact on the coupled ECMWF

1 seasonal forecasting system. *Phil. Trans. R. Soc. A*, **372**: 20130290.  
2 <http://dx.doi.org/10.1098/rsta.2013.0290>

3

4 Whartenby, WG, Quinn JC, Abarbanel HDI. 2013: The number of required observations in  
5 data assimilation for a shallow-water flow. *Mon. Wea. Rev.*, **141**, 2502-2518.

6 Xiong, X., I.M. Navon, B. Uzunoglu, 2006: A note on the particle filter with posterior  
7 Gaussian resampling. *Tellus A*, **58** (4), 456-460.

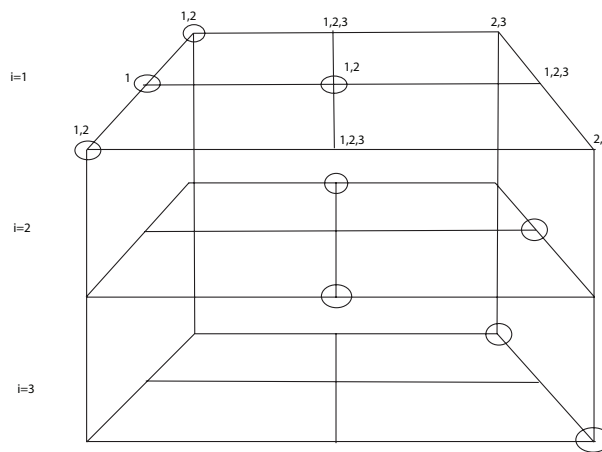
8 Yang, S.-C., E. Kalnay, B.R. Hunt, 2009: Weight interpolation for efficient data assimilation  
9 with the Local Ensemble Transform Kalman Filter. *Q. J. R. Meteorol. Soc.* **135**: 251–262.

10 Yang, S.-C., E. Kalnay, and B.R. Hunt, 2012a: Handling nonlinearity in Ensemble Kalman  
11 Filter: Experiments with the three-variable Lorenz model. *Mon. Wea. Rev.*, **in press**.  
12 Available online ([dx.doi.org/10.1175/MWR-D-11-00313.1](http://dx.doi.org/10.1175/MWR-D-11-00313.1)).

13 Yang, S.-C., E. Kalnay, and T. Miyoshi, 2012b: Improving EnKF spin-up for typhoon  
14 assimilation and prediction, *Wea. Forecasting*, **27**, 878-897.

## 15 **Figures**

16

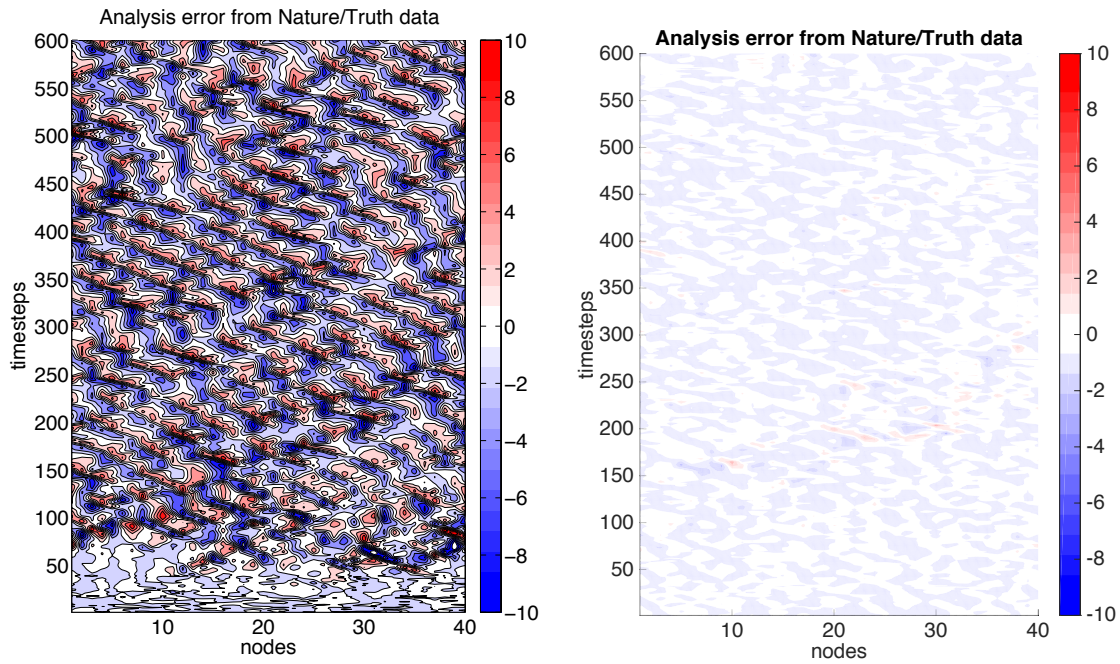


17

18 **Figure 1.** A hypothetical example depicting the construction of a single analysis member.  
19 Each level represents a different background ensemble member (particle), with a model space  
20 composed of a 3x3 grid. The nodes of the grid are circled if the member is chosen for the  
21 construction of analysis member 1 by the LPF. The numerals indicate the ids for the  
22 background members that will be averaged at the corresponding node, in this case based on  
23 the immediately adjacent neighbor points of that node.

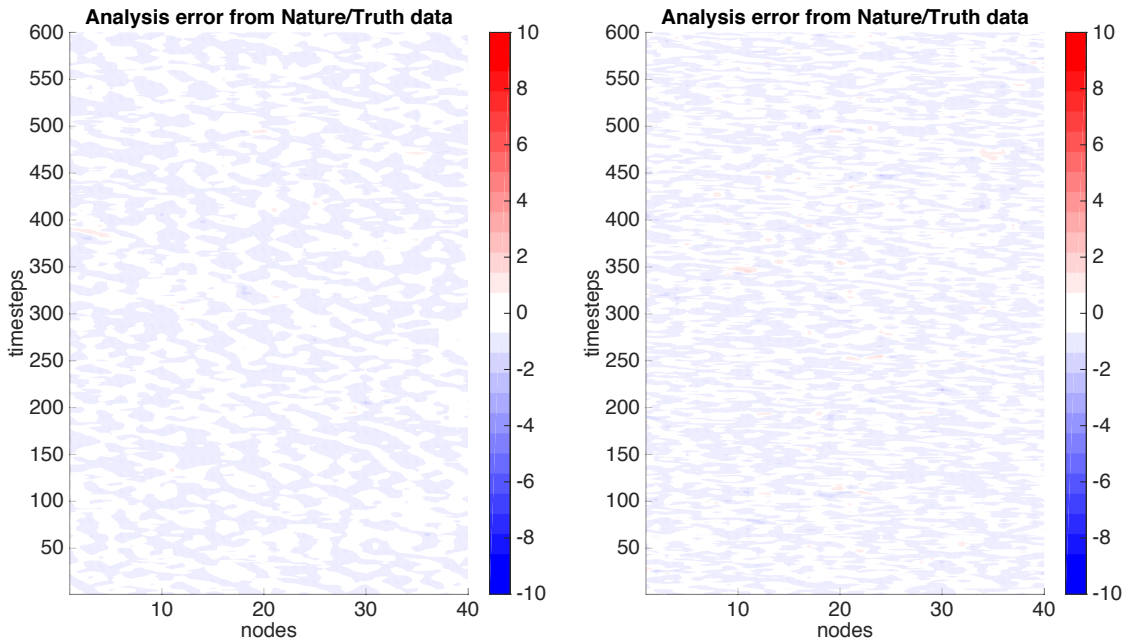


1



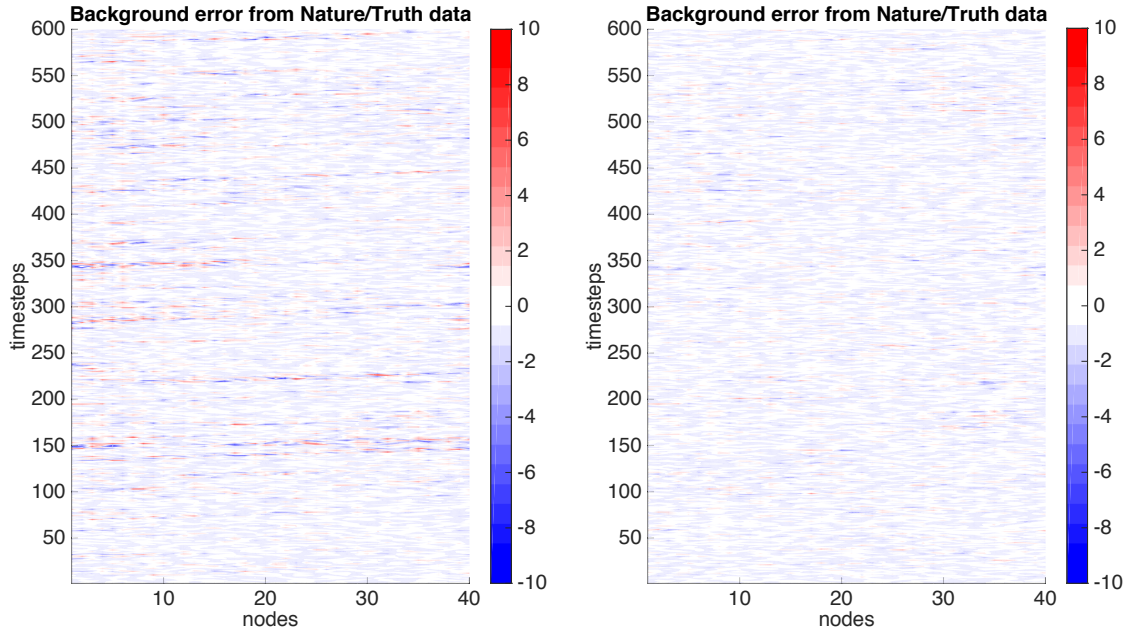
2

3 **Figure 2.** Analysis error using an analysis cycle window length  $dt=0.05$  (6-hr) for (a) the  
4 standard SIR PF using  $k=1500$  particles with  $l=20$  observations per analysis cycle, and (b)  
5 LETKF with localization radius  $r=2$ ,  $k=20$  ensemble members, and  $l=10$  observations per  
6 analysis cycle, sampled randomly on the domain.



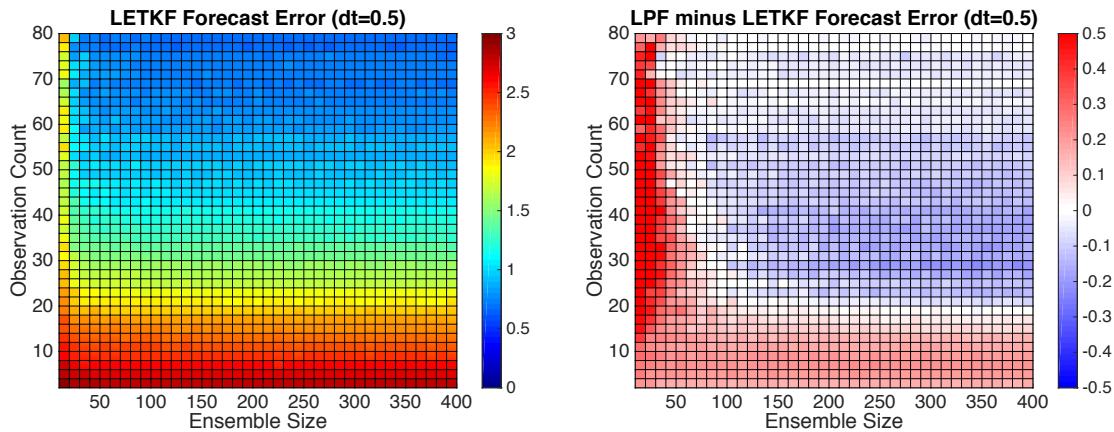
7

1 **Figure 3.** Analysis error for (a) LETKF and (b) LPF, using an analysis cycle window length  
 2  $dt=0.05$  (6-hr), localization radius  $r=2$  grid points,  $k=40$  ensemble members, and  $l=20$   
 3 observations sampled randomly on the domain (prescribed observation locations and errors  
 4 are identical for both methods).



5

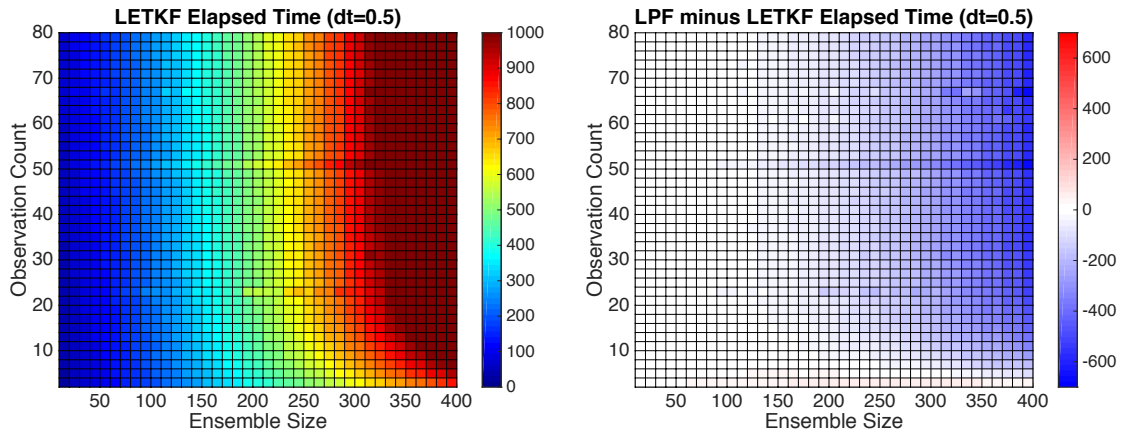
6 **Figure 4.** Forecast error for (a) LETKF and (b) LPF, using an analysis cycle window length  
 7  $dt=0.5$  (60-hr), localization radius  $r=2$  grid points,  $k=100$  ensemble members, and  $l=80$   
 8 observations sampled randomly on the domain (observation locations and errors are identical  
 9 for both methods).



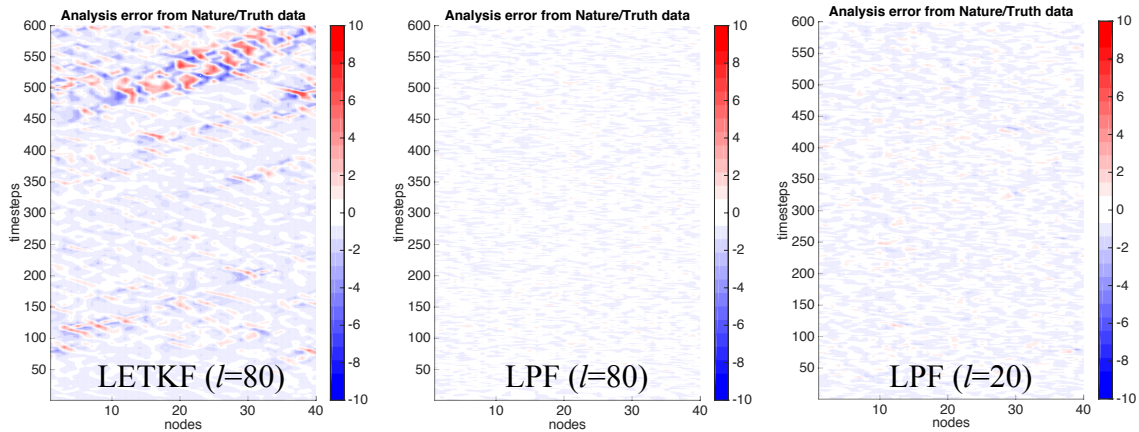
10

11 **Figure 5.** Forecast error for (a) LETKF and (b) LPF minus LETKF. LPF reduces error in  
 12 highly sampled cases with larger observation coverage. The LPF increases error in poorly

- 1 sampled cases and with low observation coverage. Each cell represents one experiment case;
- 2 absolute errors are averaged over the entire domain for 600 analysis cycles for each case.

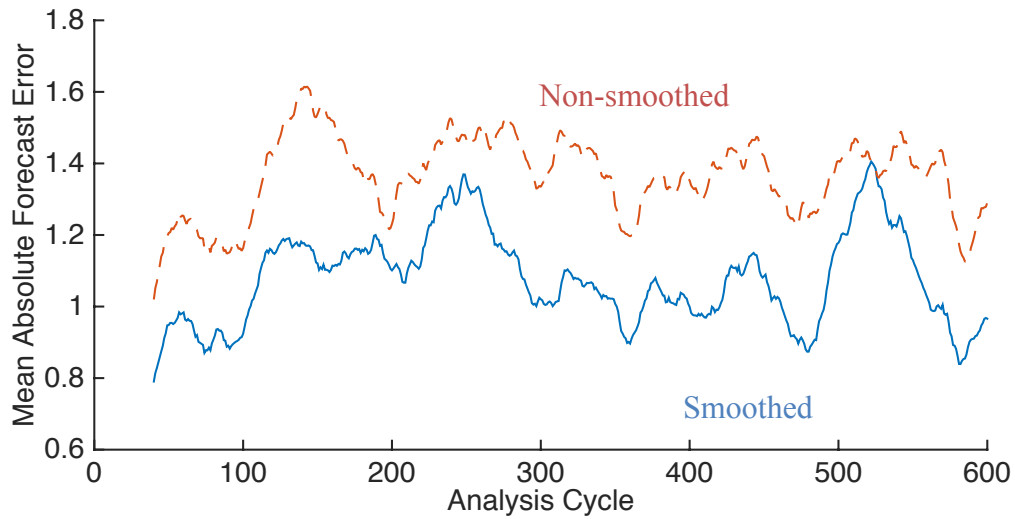


3  
4 **Figure 6.** Elapsed time in seconds for (a) LETKF and (b) LPF minus LETKF.



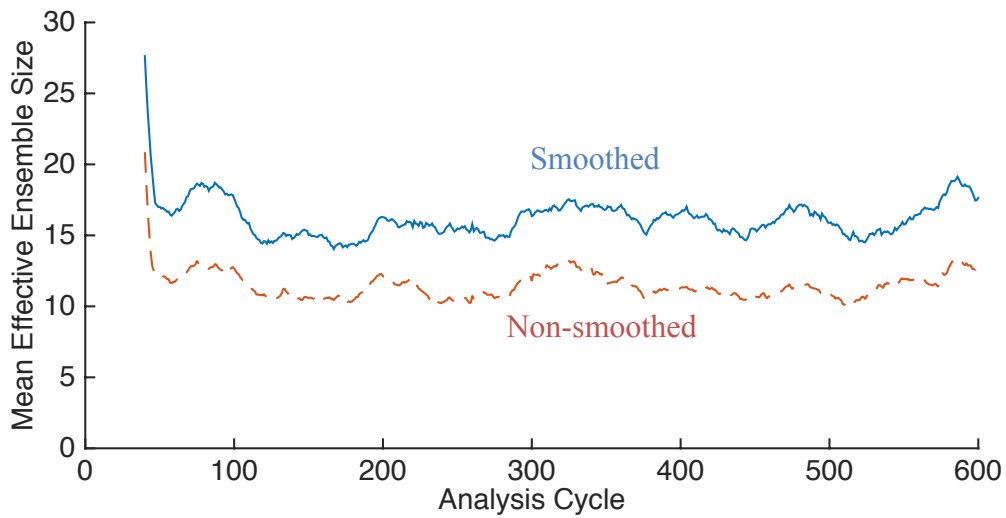
5  
6 **Figure 7.** Analysis error for (a) LETKF and (b) LPF, using  $l=80$  observations and  $k=100$   
7 ensemble members. The observations used between (a) and (b) are identical. In (c), the  
8 number of observations for LPF is reduced to  $l=20$ , but improvement in accuracy versus  
9 LETKF remains.

10



1  
 2 **Figure 8.** 40-cycle moving average of the mean absolute forecast error, comparing the Non-  
 3 smoothed (dashed red) and Smoothed (solid blue) LPF analyses. The ensemble space  
 4 smoothing improves the forecast accuracy.

5



6  
 7 **Figure 9.** Illustrating the impact of ensemble space smoothing on the effective ensemble size  
 8  $N_{eff}$ . Here we show the 40-cycle moving average of  $N_{eff}$  for the Smoothed (solid blue) and  
 9 Non-smoothed (dashed red) cases.

10